

Cell Reports, Volume 42

Supplemental information

**Biochemical and biophysical characterization
of natural polyreactivity in antibodies**

Marta T. Borowska, Christopher T. Boughter, Jeffrey J. Bunker, Jenna J. Guthmiller, Patrick C. Wilson, Benoit Roux, Albert Bendelac, and Erin J. Adams

Supplementary Materials

Figure S1. Binding of selected polyreactive mouse IgA to polyreactive ligands (Related to Figure 1) (A) Polyreactivity ELISA OD405 values of selected mouse IgA mAbs tested at different concentrations. (B) New ligands: lysozyme, ubiquitin and 50nt ssDNA, tested with Polyreactivity ELISA showing OD405 values for selected mouse IgA mAbs tested at different concentrations. Marked are also positive (3H9) and negative controls (292D8, 334B4). (C) BLI binding plot between immobilized biotinylated 25nt ssDNA and selected polyreactive mouse IgA Fabs or negative control mouse IgG 20.1 Fab vs. time.

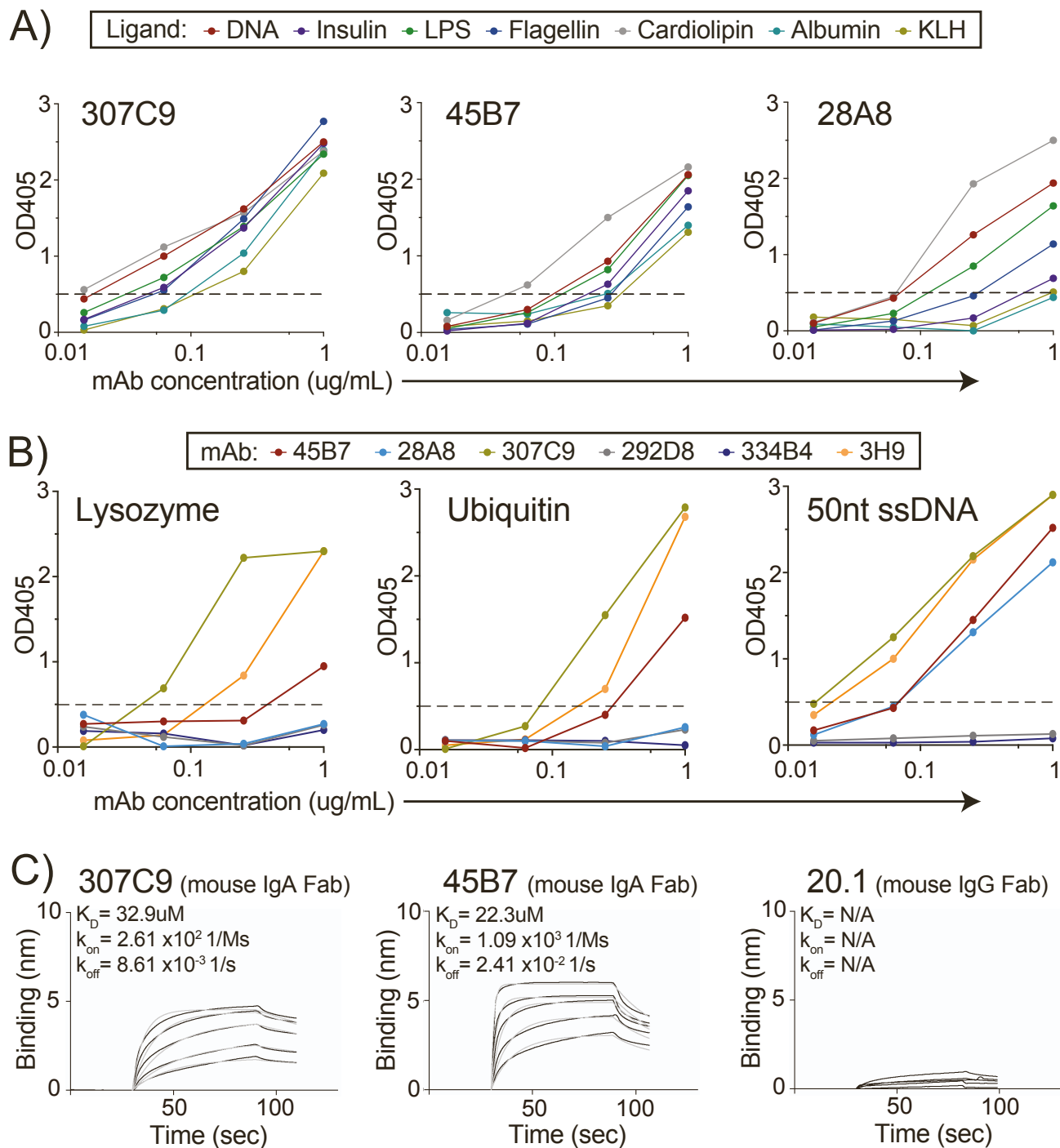


Figure S3. tICA plots and representative structures of polyreactive antibodies highlight notable rigidity of their CDR loops. (Related to Figure 4) (A) polyreactive 338E6 mouse Fab, (B) polyreactive 43G10 mouse Fab, (C) polyreactive 2G02 human Fab; Left: representative tICA plots from 1 microsecond simulations of polyreactive antibodies. Individual clusters within tICA space identify k-centers clustering are represented by colorful circles. Right: representative structures of the CDR loops from each identified cluster from tICA plots. Colors of the structures match those found in the tICA plots.

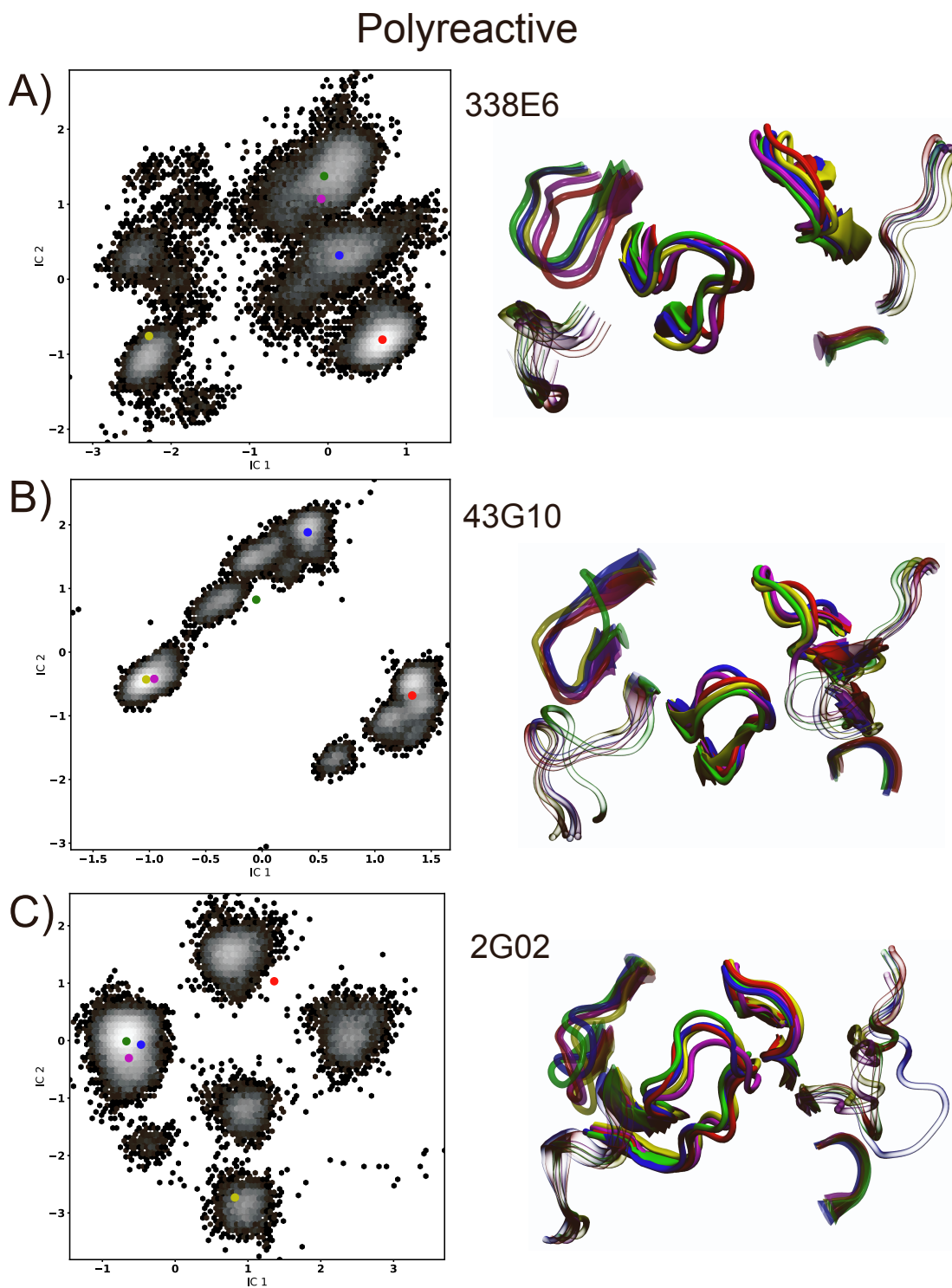


Figure S4. Root mean square deviation (RMSD) of the CDR loops of polyreactive antibodies throughout 1 μ s simulations show limited dynamics in CDR3H and CDR2H. (Related to Figure 4) RMSD traces for polyreactive 338E6, 43G10 and 2G02 Fabs, over all simulated time across four of the six CDR loops. Key differences in the dynamics across poly- and monoreactive antibodies can be found within the heavy chain and CDR L1.

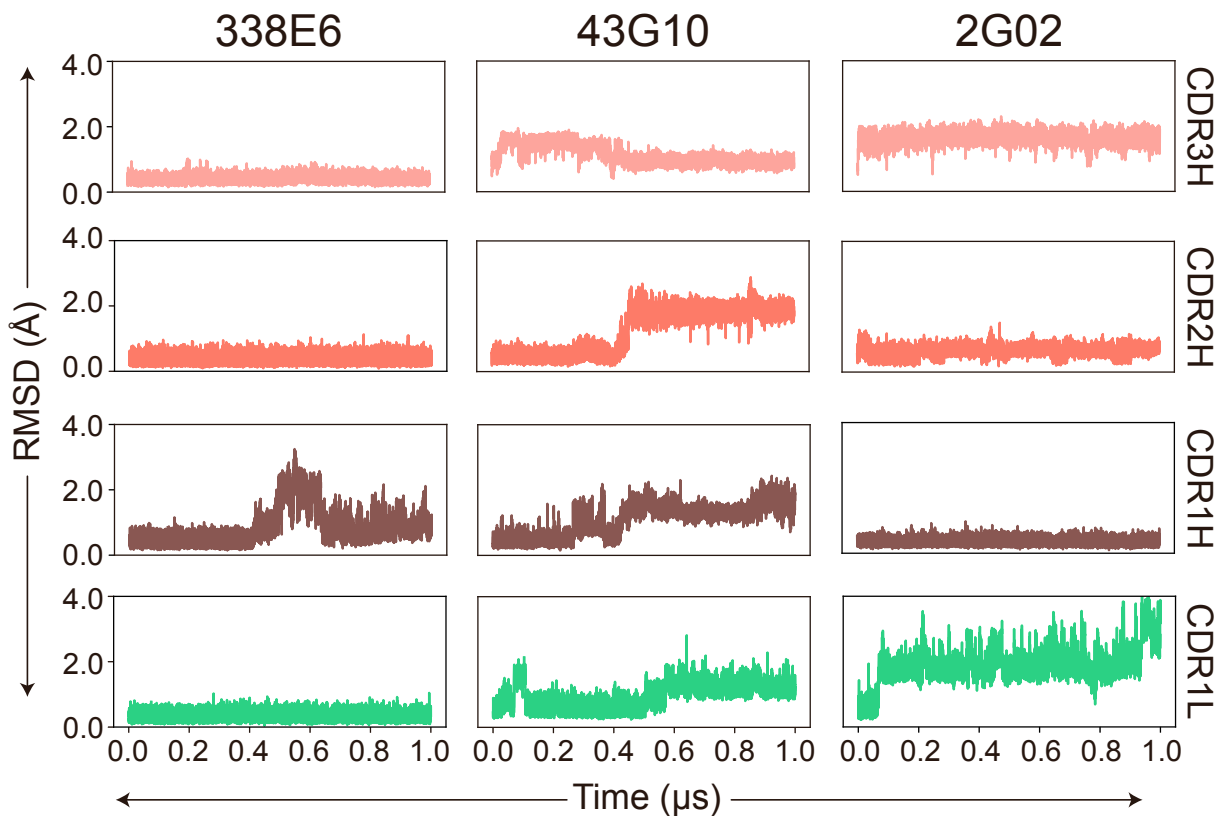


Figure S5. Root mean square fluctuations (RMSF) measured over simulation triplicates show similar behavior independent of initial velocity assignments (Related to Figure 4). Each column is associated with polyreactive 338E6, 43G10 or 2G02 Fab structure, while each row corresponds to the RMSF of either CDR3H (top), CDR1L (middle), or CDR3L (bottom). Replicas are colored according to the key in the middle column.

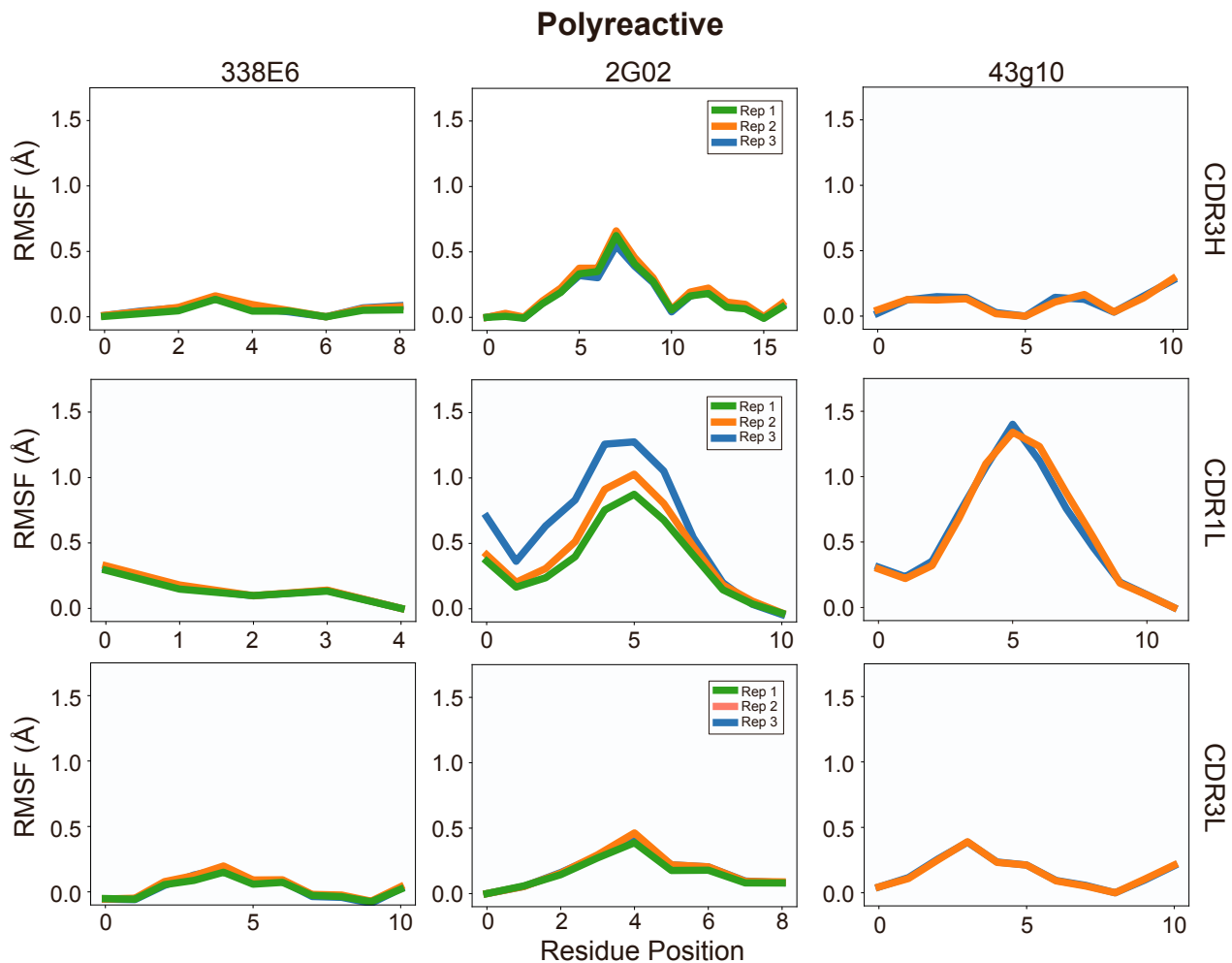


Figure S6. tICA plots and representative structures of monoreactive/ reduced polyreactivity antibodies highlight exceptional flexibility of their CDR loops (Related to Figure 4). (A) monoreactive 4C05 human Fab, (B) monoreactive 3B03 human Fab, (C) reduced polyreactivity 2G02 mutant human Fab; Left: representative tICA plots from 1 microsecond simulations of monoreactive antibodies. Individual clusters within tICA space identify k-centers clustering are represented by colorful circles. Right: representative structures of the CDR loops from each identified cluster from tICA plots. Colors of the structures match those found in the tICA plots.

Non-Polyreactive/ Reduced Polyreactivity

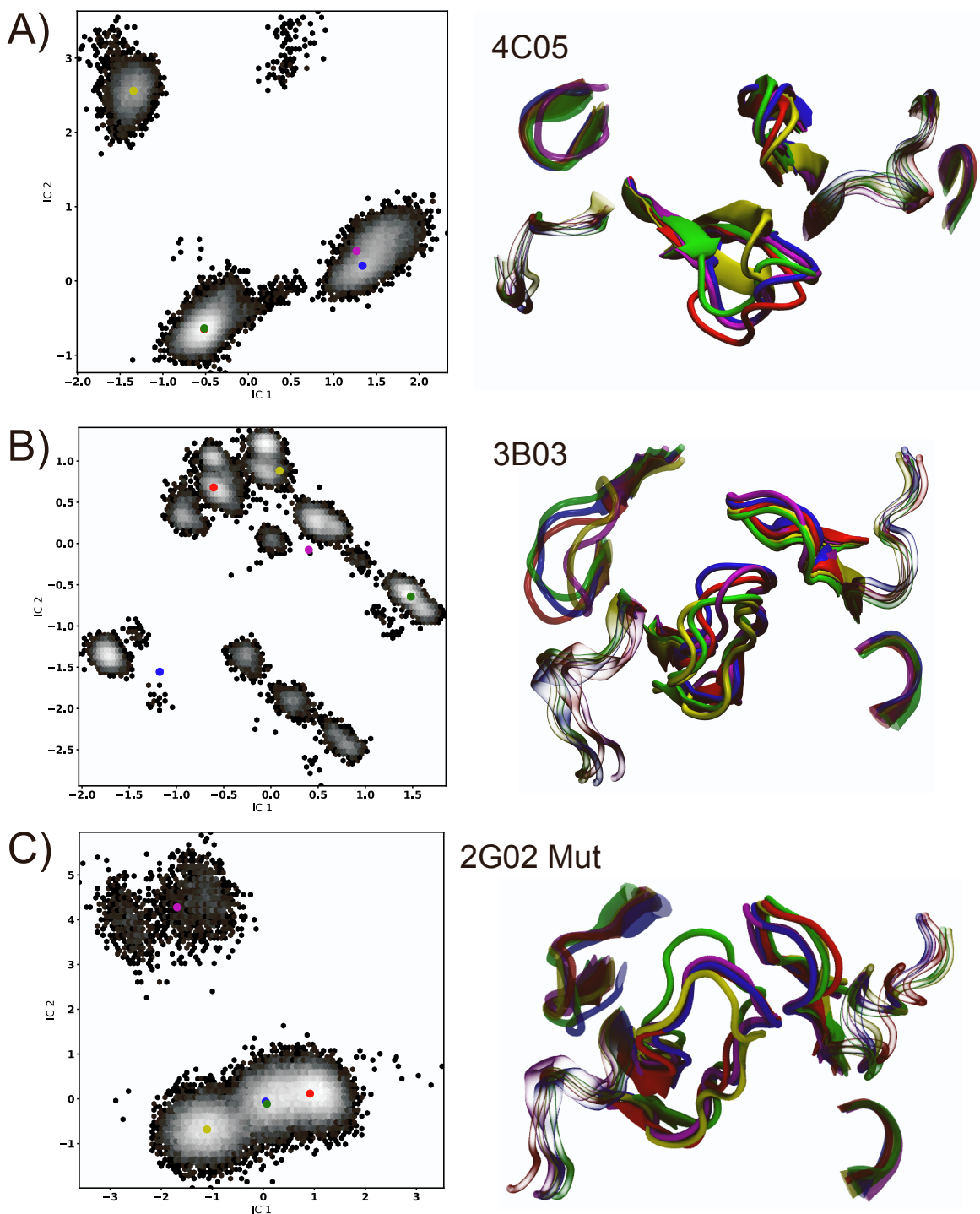


Figure S7. Root mean square deviation (RMSD) of the CDR loops of monoreactive/reduced polyreactivity antibodies throughout 1 μ s simulations show high flexibility in CDR3H and CDR2H (Related to Figure 5). RMSD traces for monoreactive 4C05, 3B03 and 2G02 mutant Fabs, over all simulated time across four of the six CDR loops. Key differences in the dynamics across polyreactive and monoreactive antibodies can be found within the heavy chain and CDR L1.

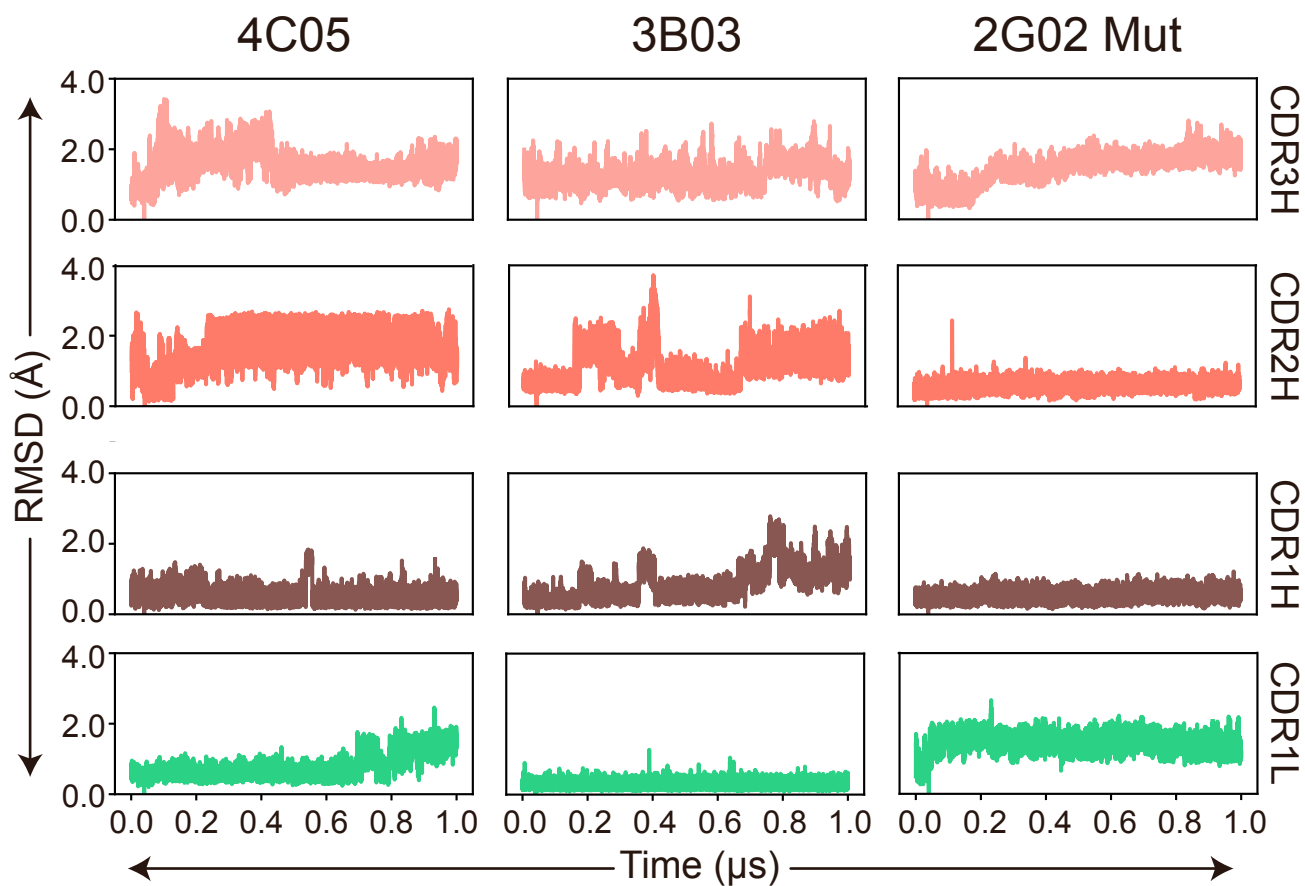


Figure S8. Root mean square fluctuations (RMSF) measured over simulation triplicates show similar behavior independent of initial velocity assignments (Related to Figures 4,5). Each column is associated with monoreactive 4C05, 3B03 Fab structures and reduced polyreactivity 2G02 mutant model based on 2G02 wildtype Fab structure, while each row corresponds to the RMSF of either CDR3H (top), CDR1L (middle), or CDR3L (bottom). Replicas are colored according to the key in the central column.

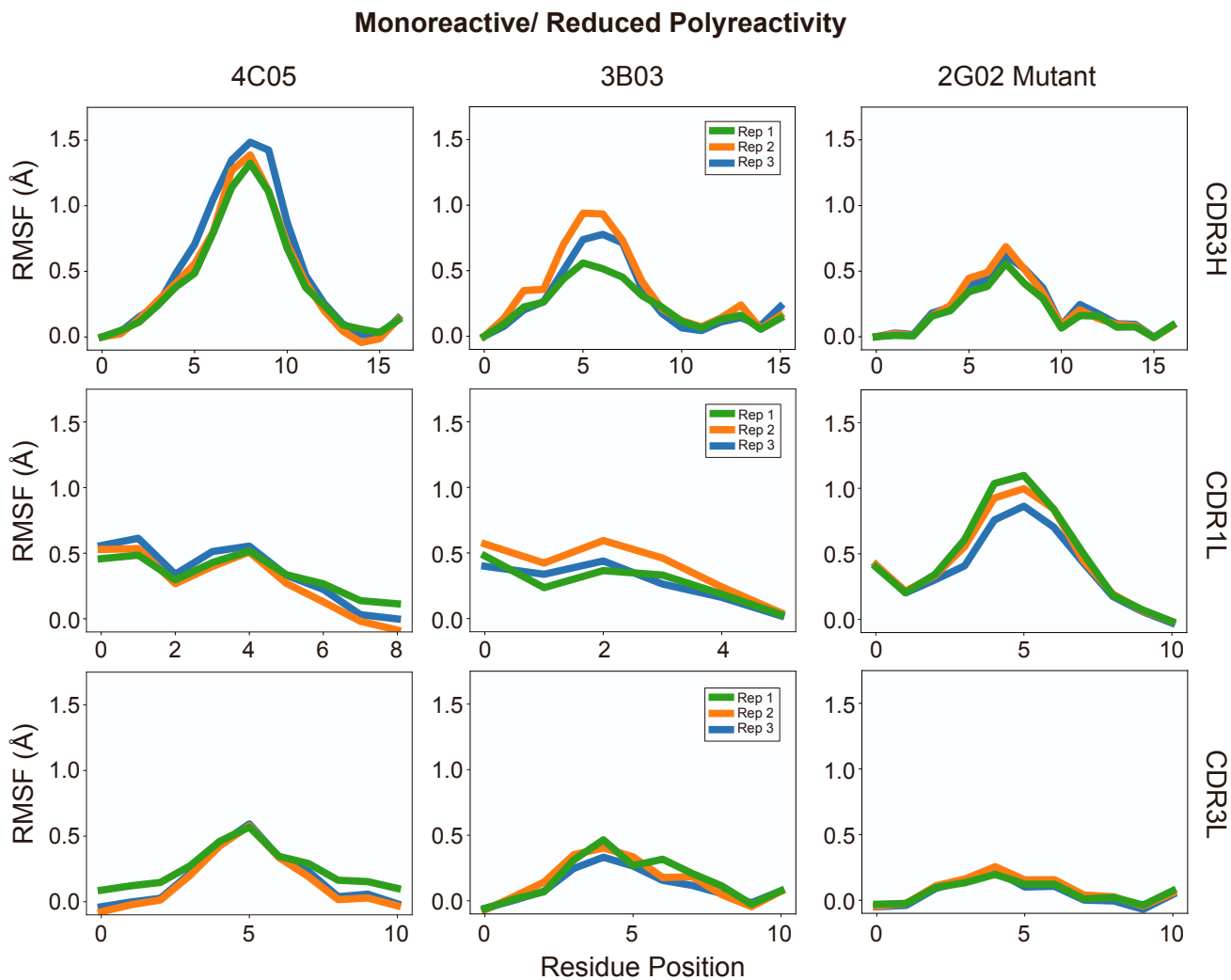


Figure S9. Root mean square deviation (RMSD) of the CDR loops of additional polyreactive antibodies throughout 300ns simulations show low flexibility in CDR3H and CDR2H (Related to Figures 4,5). RMSD traces for polyreactive CR9114, 1F02, CH65 and F16 Fabs, over all simulated time across four of the six CDR loops. Key differences in the dynamics across polyreactive and monoreactive antibodies can be found within the heavy chain and CDR L1.

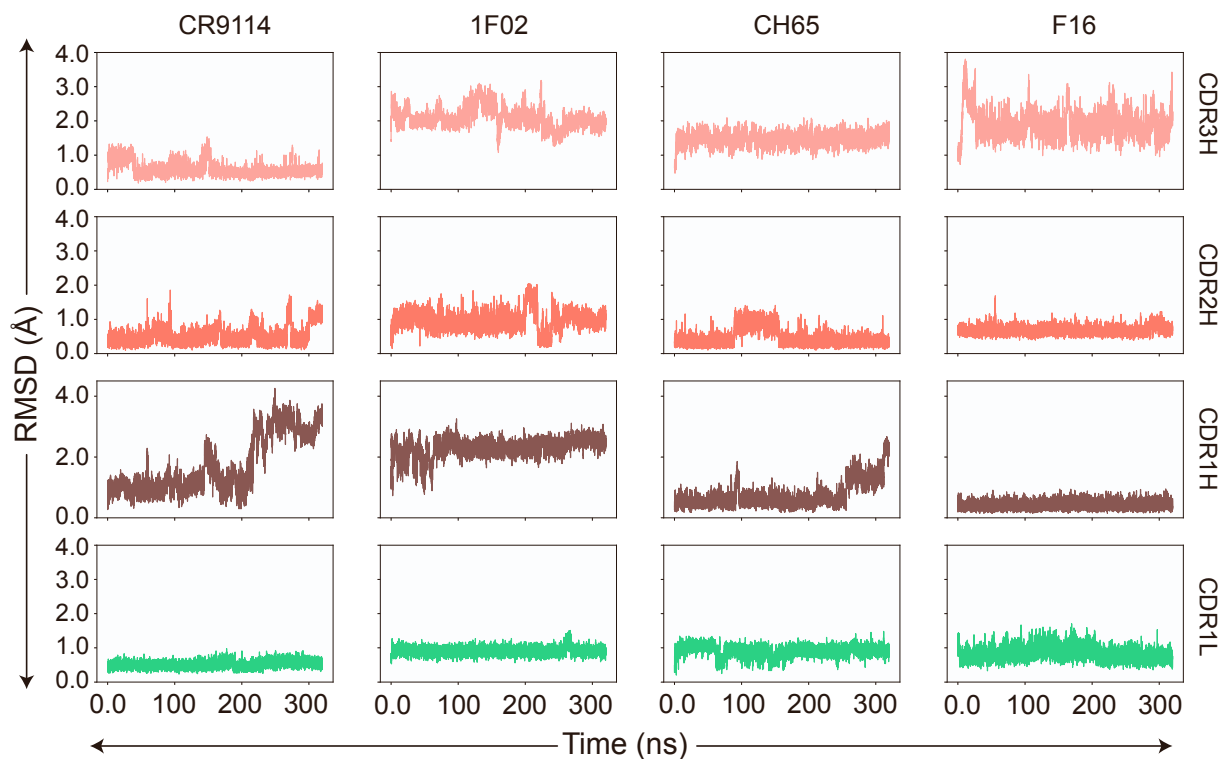


Figure S10. Root mean square fluctuation (RMSF) of the CDR loops across all simulated antibodies show clear trends in (A) CDR3H and (B) CDR3L flexibility (Related to Figures 4,5). The presented RMSF is a bootstrapped average over triplicate trajectories for each antibody, with the standard deviation given as shaded regions about this average. Asterisks identify statistically significant differences ($p < 0.05$) calculated using a non-parametric permutation test (Methods). Polyreactive antibodies are represented by blue markers with light blue standard deviation shading, while monoreactive antibodies are represented by red markers with light red standard deviation shading. The 2G02 mutant with reduced polyreactivity is represented by purple markers with light purple standard deviation shading. To align RMSF traces of CDR loops of different size, the most flexible residue (by RMSF) within the CDR loop is set to a residue position of 0, and the RMSF of each previous or subsequent residue is plotted in order.

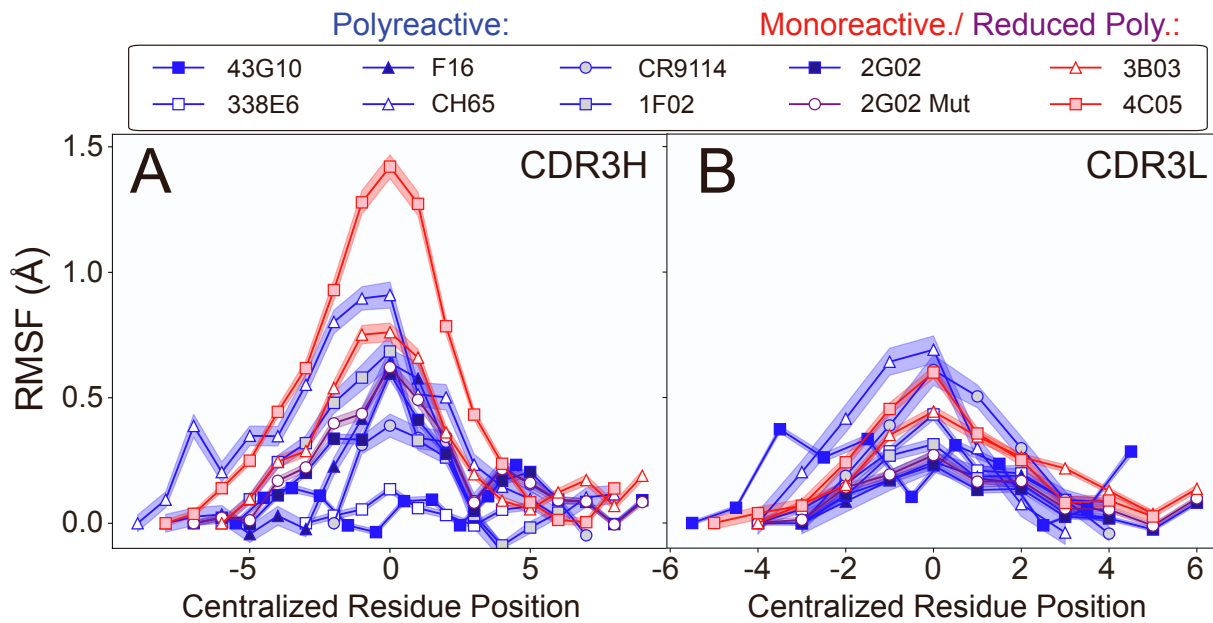


Figure S11. Root mean square fluctuation (RMSF) of the CDR loops averaged across all simulated antibodies show statistically significant trends in (left) CDR3H and (middle) CDR3L, but not CDR1L (right), flexibility (Related to Figures 4,5). The presented RMSF is a bootstrapped average over triplicate trajectories with all polyreactive or monoreactive antibodies pooled into a singular dataset (see Methods for more details). The standard deviation given as shaded regions about this average. Asterisks identify statistically significant differences ($p < 0.05$) calculated using a non-parametric permutation test (Methods). Polyreactive antibodies are represented by blue markers with light blue standard deviation shading, while monoreactive antibodies are represented by red markers with light red standard deviation shading. To pool RMSF from CDR loops of different size, the contiguous 5 residue region with the highest flexibility from each antibody is taken for the RMSF calculation.

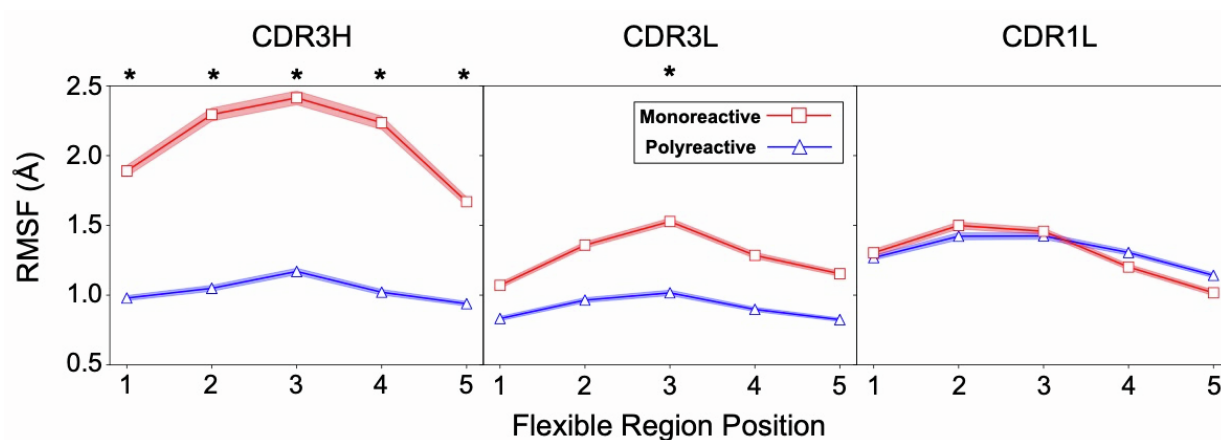


Table S1. Data collection and refinement statistics of polyreactive 338E6, 43G10, 2G02, and monoreactive 3B03, 4C05 Fab structures.

	338E6 Fab	43G10 Fab	2G02 Fab	3B03 Fab	4C05 Fab
Wavelength	40.61 - 1.83 (1.895 - 1.83)	57.88 - 1.634 (1.692 - 1.634)	69.33 - 1.67 (1.73 - 1.67)	64.12 - 1.632 (1.69 - 1.632)	37.76 - 1.77 (1.833 - 1.77)
Resolution range	P 1 21 1	P 21 21 21	P 1 21 1	P 1	C 1 2 1
Space group	40.92.59.65 82.2502 90 99.1 90	62.2399 108.47 115.75 90 90 90	70.1598 59.44 99.2799 90 98.8301 90	52.4198 66.17 90.2383 104.09 93.31 91.6	79.8391 70.6089 87.6797 90 108.95 90
Unit cell	188893 (106048)	2239885 (187748)	1750561 (16892)	903633 (90390)	84718 (8470)
Total reflections	33933 (3289)	97569 (9583)	92961 (9082)	132793 (13000)	44090 (4398)
Unique reflections	32.1 (31.9)	23.0 (19.5)	1.9 (1.9)	6.8 (6.8)	1.9 (1.9)
Multiplicity	97.38 (95.53)	99.33 (95.12)	96.38 (87.99)	88.47 (88.66)	98.04 (98.81)
Completeness (%)	21.60 (4.97)	18.90 (0.55)	7.22 (2.10)	27.55 (1.42)	11.61 (4.82)
Mean I/sigma(I)	14.95	26.58	16.28	21.81	18.34
Wilson B-factor	0.7016 (1.134)	0.7845 (7.964)	0.1468 (1.662)	0.5797 (1.552)	0.02884 (0.134)
R-merge	0.7129 (1.153)	0.8025 (8.182)	0.2076 (2.35)	0.6379 (1.698)	0.04079 (0.1896)
R-meas	0.1241 (0.2033)	0.1657 (1.844)	0.1468 (1.662)	0.2612 (0.6786)	0.02884 (0.134)
R-pim	0.903 (0.731)	0.741 (0.0942)	0.943 (0.171)	0.648 (0.318)	0.998 (0.924)
CC1/2	0.974 (0.919)	0.923 (0.415)	0.985 (0.541)	0.887 (0.695)	1 (0.98)
CC*	33772 (3289)	96977 (9162)	90525 (8203)	129063 (12974)	44088 (4398)
Reflections used in refinement	1689 (167)	4874 (445)	1936 (170)	2000 (196)	2099 (190)
Reflections used for R-free	0.1748 (0.2049)	0.2197 (0.4006)	0.1926 (0.2742)	0.2020 (0.3247)	0.1870 (0.2160)
R-work	0.1791 (0.2263)	0.2378 (0.4037)	0.2198 (0.3135)	0.2338 (0.3379)	0.2192 (0.2451)
R-free	0.758 (0.598)	0.796 (0.372)	0.957 (0.549)	0.800 (0.638)	0.960 (0.879)
CC(work)	0.683 (0.636)	0.797 (0.251)	0.956 (0.625)	0.770 (0.658)	0.940 (0.850)
CC(free)	3705	3564	7374	7302	3632
Number of non-hydrogen atoms	3243	3391	6654	6435	3281
macromolecules	462	173	720	867	351
solvent	425	441	869	849	433
Protein residues	0.006	0.007	0.007	0.006	0.007
RMS(bonds)	0.89	0.92	1	0.88	1.02
RMS(angles)	96.9	97.46	98.02	96.77	96.97
Ramachandran favored (%)	3.1	2.31	1.86	3.23	2.8
Ramachandran allowed (%)	0	0.23	0.12	0	0.23
Ramachandran outliers (%)	0	0.77	0.4	0	0.27
Rotamer outliers (%)	3.13	1.94	5.79	3.63	4.48
Clashscore	17.29	37.71	20.11	29.32	24.35
Average B-factor	16.45	37.52	19.33	28.42	23.71
macromolecules	23.16	41.52	27.29	36.03	30.41
solvent					

(Statistics for the highest-resolution shell are shown in parentheses.)